

MIC Impact on Mechanical Property Degradation of X80 Pipeline Steel by A Sulfate Reducing Bacterium

Zhong Li, Jike Yang
Dept. of Chemical & Biomolecular Eng.
Inst. for Corrosion & Multiphase Tech.
Ohio University
Athens, OH 45701, USA

Magdy E. Mohamed, Mazen A. Saleh
Research and Development Center,
Saudi Arabian Oil Company
Dhahran 31311, Saudi Arabia

Sith Kumseranee, Suchada Punpruk
PTTEP
Chatuchak, Bangkok 10900, Thailand

Tingyue Gu (gu@ohio.edu)
Dept. of Chemical & Biomolecular Eng.
Inst. for Corrosion & Multiphase Tech.
Ohio University
Athens, OH 45701, USA

ABSTRACT

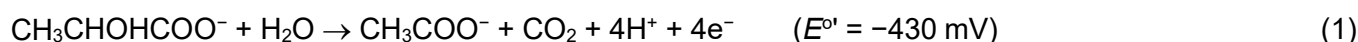
Apart from pinhole leaks, MIC (microbiologically influenced corrosion) can also cause catastrophic failures such as pipe rupture and support beam collapse due to mechanical strength degradation or stress corrosion cracking. In this work, X80 pipeline steel dogbone coupons and square coupon were immersed in 150 mL *Desulfovibrio vulgaris* (a sulfate reducing bacterium or SRB) broths for up to 14 days. The headspace volumes in the anaerobic bottles were varied from 150 mL to 300 mL to increase MIC severity. After 14 days of incubation at 37°C, the sessile cell counts were 6.5×10^7 cells/cm² for 150 mL, 2.3×10^8 cells/cm² for 200 mL and 1.4×10^9 cells/cm² for 300 mL headspace volumes, respectively owing to reduced H₂S toxicity in the broth with a larger headspace. Weight losses were 1.7 mg/cm², 1.9 mg/cm² and 2.3 mg/cm² for 150 mL, 200 mL 300 mL headspace volumes, respectively. The corresponding pit depths were 2.6 μm, 4.2 μm and 6.2 μm for 150 mL, 200 mL and 300 mL headspace volumes, respectively. Electrochemical impedance spectroscopy (EIS), linear polarization resistance (LPR) and potentiodynamic polarization results corroborated the increasing weight loss and pitting data trends. Tensile testing after the 14-day immersion indicated that more severe MIC pitting led to a higher ultimate strain loss by up to 22%, while the ultimate strength losses for all headspace volumes were quite small (5% and below).

Key words: MIC, mechanical property, sulfate reducing bacteria, tensile test, H₂S.

INTRODUCTION

MIC has become a major concern in marine, oil and gas, and water utilities industries, etc. MIC accounts for 20% of all of corrosion losses.¹ Walsh estimated that MIC leads to substantial financial losses of approximately \$30-50 billion per year in the US.² In addition to pinhole leaks, MIC can cause mechanical property degradation, leading to metal fracturing/rupturing and cracking that reduce equipment service lifespan.³ Most MIC studies so far focused on pitting corrosion. There is a lack of studies on the impacts of MIC on mechanical property degradation. In practical applications, disastrous consequences such as pipeline rupture and support beam collapse can be caused by mechanical property degradation due to MIC.

SRB are a major type of microbes that cause MIC. SRB can acquire energy by oxidizing organic substances or H₂ while reducing sulfate (SO₄²⁻) to hydrogen sulfide (H₂S) and other sulfide species.⁴ When sulfate acts as the electron acceptor and lactate (soluble) as the electron donor for SRB respiration, the redox reaction occurs entirely in the SRB cytoplasm to generate energy.⁵



In these two reactions, E° is the reduction potential (vs. SHE) at 25 °C, pH 7, and 1 M solutes (or 1 bar gases). SRB sessile cells require energy to maintain themselves. When there is a lack of carbon source in the local environment near the bottom of an SRB biofilm, elemental iron can provide the electrons for SRB survival, which leads to MIC. E° of Fe²⁺/Fe is similar to that of acetate + CO₂/lactate.⁶ This means elemental Fe is as energetic as lactate for SRB.



Therefore, the cell potential (ΔE°) of the redox reaction combining Reactions (3) and (2) above is +230 mV, which results in a negative Gibbs free energy change, indicating that the overall corrosion reaction is thermodynamically favored.⁷ Electrons from extracellular iron (insoluble) oxidation must be transported across the SRB cell wall to the SRB cytoplasm for sulfate reduction. This kind of electron transfer process is known as extracellular electron transfer (EET), an important topic in microbial metabolism for energy production.⁴ *D. vulgaris* MIC of carbon steel observes the EET-MIC theory according to the evidence provided by carbon source starvation tests and electron mediator tests in the literature^{5, 8, 9}. Experimental data have rather conclusively shown that H₂S is not the cause of *D. vulgaris* (a typical SRB strain) corrosion of carbon steel at near neutral broth pH.⁹ Typical SRB MIC tests are not like abiotic H₂S corrosion which involves acidic pH.

X80 carbon steel is widely used in many industries because of their low cost and ease of fabrication. However, X80 steel pipelines may suffer from both MIC and mechanical property degradation caused by MIC. This study investigated the effects of SRB on MIC and the subsequent mechanical property degradation of X80 pipeline steel.

In the past, most investigations focused on MIC pitting only. Not many studies paid attention to the MIC effects on the degradation of mechanical properties. MIC pitting of metal surfaces weaken the metals.⁹⁻¹⁴ Pit density and depth both impacted the mechanical properties of materials such as elongation.¹⁵ In abiotic corrosion studies, Saad-Eldeen et al. found that corrosion activity degraded the ultimate strength of steel.¹⁶ It is suggested that when SRB are present, some engineering materials are likely to fail in a relatively shorter time than in an abiotic environment.¹⁷ One study showed that the ultimate strength and ultimate strain were reduced significantly in the presence of the *Pseudomonas* species due to the biofilm formation and the resultant MIC process.¹⁸ In another study, the presence of corrosive *Bacillus megaterium* bacterium adversely decreased the mechanical parameters such as yield stress, ultimate strength and elongation of an Al-Cu alloy.¹⁹

It has been known that in carbon steel MIC by SRB, a larger headspace allows more H₂S to escape from

the broth. This reduces the H₂S toxicity in the broth, allowing better planktonic and sessile SRB growth, and thus leading to more severe MIC.¹² In this study, dogbone coupons made of X80 carbon steel were used to investigate mechanical property degradation as a consequence of exposure to varied severity of MIC pitting by SRB, which was achieved by varying the headspace. After SRB exposure in anaerobic bottles, X80 dogbones were analyzed for MIC pitting and then tested on a tensile machine to measure mechanical property damages. Square X80 coupons were used to obtain weight loss. Square X80 coupons were also used as working electrodes in electrochemical glass cells to measure MIC severity electrochemically to corroborate weight loss and pit depth data trends from anaerobic bottles and to provide transient corrosion behavior.

EXPERIMENTAL PROCEDURE

X80 steel composition is listed in Table 1. Dogbone coupons were too heavy to measure milligram weight loss accurately. Thus, three square coupons, each with a 1 cm² unpainted top surface (all other surfaces were covered with a polytetrafluoroethylene paint), were incubated in each anaerobic bottle to obtain one MIC weight loss data point. Square coupons (1 cm² exposed surface) were also used as working electrodes in electrochemical glass cells. Dogbone specimens are widely used to test the mechanical property of metal materials.²⁰ The dimensions of the dogbone coupons (Figure 1b) were based on the ASTM E8-04 standard. The dogbone coupons were polished to 1200 grit by the supplier. Each dogbone coupon was painted with Teflon, except for a middle section with a width of 6 mm and length of 22 mm which was exposed upward to the broth. The surfaces of all the square coupons (including the abiotic control and electrode coupons) were sequentially polished with 180, 400 and 600 grit abrasive papers. After that, all the coupons were cleaned with pure isopropanol and dried under UV light for 20 minutes.

Table 1
Composition of X80 steel

Element	C	Mn	Ni	Cu	Si	Mo	Cr	Nb	Ti	Fe
Amount (wt%)	0.050	1.850	0.285	0.246	0.228	0.307	0.016	0.065	0.013	balance

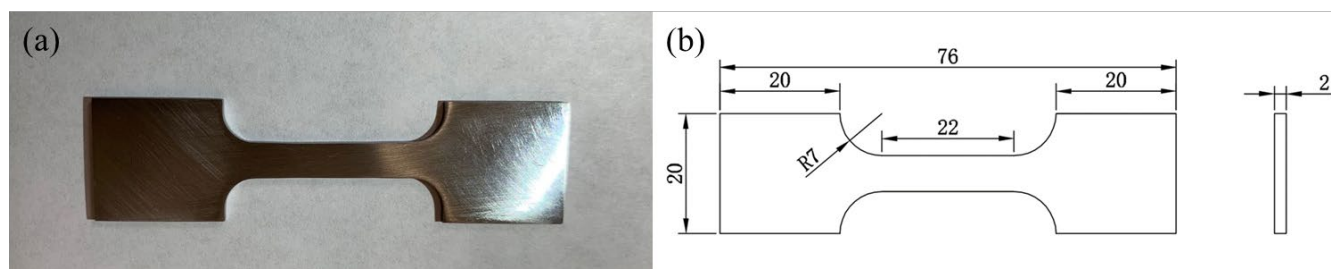


Figure 1. (a) dogbone coupon of X80 steel, and (b) coupon dimensions in mm.²¹

D. vulgaris (ATCC[†] 7757 strain), a common SRB strain in MIC research, was selected for this research. The culture medium was ATCC[†] 1249 medium, which is a modified Baar's medium for sulfate reducers. The culture medium pH was adjusted to pH 7 using a NaOH solution. Dogbone coupons were immersed in anaerobic bottles with 150 mL culture medium and varied headspace volumes (150 mL, 200 mL and 300 mL). The headspace variation was achieved using different bottle sizes and inert glass beads as filler to reduce the available volume. The anaerobic bottles with culture medium were sterilized in an autoclave at 121 °C for 40 minutes. After autoclaving, the SRB culture medium was deoxygenated using filter-sterilized N₂ sparging for more than 45 minutes. One hundred ppm (final) L-cysteine was then added to the culture medium as an oxygen scavenger to reduce dissolved oxygen further and to mitigate any possible oxygen leakage. Each bottle was inoculated with 2 mL SRB seed culture. The abiotic control dogbone coupon was immersed in an anaerobic bottle with 150 ml culture medium and 150 mL headspace without SRB inoculation. Each bottle contained one dogbone coupon. For the weight loss measurement, each bottle contained 3 square coupons.

The concentration of H₂S in the headspace and total pressure in each anaerobic bottle were measured

[†]Trade name
© 2024 Association for Materials Protection and Performance (AMPP). All rights reserved. No part of this publication may be reproduced, stored in a retrieval system, or transmitted, in any form or by any means (electronic, mechanical, photocopying, recording, or otherwise) without the prior written permission of AMPP.

Positions and opinions advanced in this work are those of the author(s) and not necessarily those of AMPP. Responsibility for the content of the work lies solely with the author(s).

using a portable H₂S sensor (Model GAXT-H-DL, BW Technologies, Calgary, Alberta, Canada), a digital manometer (Model Xplorer GLX - PS-2002, PASCO scientific, Roseville, CA, USA), respectively. The H₂S sensor has an upper limit of 100 ppm (v/v). If a headspace sample had a higher concentration, dilution was required.⁹

After 14 days of incubation, the X80 square coupons and dogbone coupons were retrieved. The biofilms and corrosion products on the coupon surfaces were removed using a fresh Clarke's solution according to ASTM G1–03 before weighing. After the removal, the maximum pit depth for each dogbone coupon was obtained under an infinite focus microscopy (IFM) machine (Model ALC13, Alicona Imaging GmbH, Graz, Austria). After the pit depth analysis, tensile tests were performed on an electromechanical universal testing machine (E44.304, MTS system, MN, USA) on the same dogbone coupons. The square coupons were cleaned with the Clarke's solution before weighing.

A potentiostat (Model VersaSTAT 3, Princeton Applied Research, Oak Ridge, TN, USA) was used to measure the electrochemical responses of the X80 working electrode (1 cm²) in SRB broth. Each glass cell contained 150 mL deoxygenated culture medium (fixed) with either 150 mL, 200 mL or 300 mL headspace (adjusted using inert glass beads). Each glass cell was inoculated with 2 mL SRB seed culture before incubation at 37°C. A saturated calomel electrode (SCE) was used as the reference electrode, and a platinum plate (10 mm × 10 mm × 1 mm) was used as the counter electrode. The abiotic control working electrode was immersed in an anaerobic bottle with 150 mL culture medium and 150 mL headspace without SRB inoculation. There was no need to vary the headspace for the abiotic control because H₂S escape to the headspace would not occur abiotically. Open circuit potential (OCP), LPR, EIS and potentiodynamic polarization analyses were performed. LPR was scanned at a rate of 0.1667 mV/s in the range of –10 mV to +10 mV vs. OCP. EIS was performed at OCP by applying a sinusoidal voltage signal of 10 mV (amplitude) in the frequency ranging from 10⁴ to 10⁻² Hz. Potentiodynamic polarization curves were measured at the end of the 14-day incubation from OCP to OCP – 200 mV using one working electrode and from OCP to OCP + 200 mV using another working electrode in a different glass cell at a rate of 0.1667 mV/s. The corrosion potential (E_{corr}), corrosion current density (i_{corr}), and anodic and cathodic Tafel slopes (β_a and β_c) were determined from a Tafel analysis of the polarization curves.

RESULTS AND DISCUSSION

Table 2 shows that the H₂S concentrations in the headspace gas phase for the anaerobic bottles (each containing one dogbone coupon) with headspace volumes of 150 mL, 200 mL and 300 mL were 8.50 × 10³ ppm (v/v), 7.75 × 10³ ppm, and 7.28 × 10³ ppm, respectively after the 14-day incubation. The corresponding H₂S concentration in the liquid phase was estimated based on H₂S equilibrium at 37°C according to Ning et al.²² The dissolved [H₂S] in the culture medium in the anaerobic bottles with headspace volumes of 150 mL, 200 mL and 300 mL were 1.06 mM, 0.95 mM and 0.84 mM, respectively (Figure 2 and Table 2). As expected, a larger headspace allowed more H₂S (Table 2) to escape from the liquid phase in order to reach a different H₂S equilibrium between the gas and liquid phases. Figure 2 also shows that the final broth pH values were 7.08, 7.26, and 7.54 corresponding to headspace volumes of 150 mL, 200 mL and 300 mL, respectively. pH increased with the increasing headspace volume, because a larger headspace allowed more H₂S to escape and this takes away more protons from the broth as shown in Reaction (4).¹² According to the literature,¹² a *D. vulgaris* broth in an anaerobic vial usually has near neutral pH because its normal metabolism does not change the scalar or vectorial proton concentration.



Table 2
H₂S pressure in headspace and calculated H₂S concentration in 150 mL broth

Headspace volume (mL)	H ₂ S in headspace (10 ³ ppm) (v/v)	Headspace pressure (bar)	H ₂ S partial pressure (10 ⁻² bar)	[H ₂ S] in broth (mM)	H ₂ S in headspace (10 ⁻⁴ mol)	Total H ₂ S in bottle (10 ⁻⁴ mol)
150	8.50	1.70	1.44	1.06	0.84	0.99
200	7.75	1.66	1.29	0.95	1.00	1.14
300	7.28	1.58	1.15	0.84	1.34	1.47

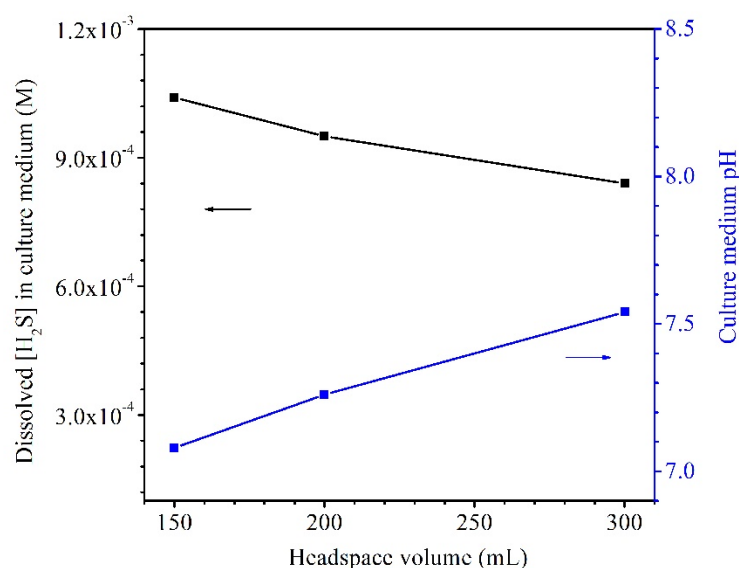


Figure 2. Dissolved [H₂S] in both and broth pH after 14-day incubation in bottles with fixed 150 mL broth and varied headspace volume.

The dissolved [H₂S] in the broth became lower with the increasing headspace volume while the pH value became higher (Table 2 and Figure 2). All the pH values in this work were above but close to 7. This is different from abiotic H₂S corrosion studies, in which researchers introduce exogenous H₂S to an aqueous solution resulting in an acidic pH.²³

After the 14-day incubation, the sessile cell count was found to be higher in the anaerobic bottle with a larger headspace volume (Figure 3). The cell counts on coupons in the bottles with the headspace volumes of 150 mL, 200 mL and 300 mL were 6.5 × 10⁷ cells/cm², 2.3 × 10⁸ cells/cm² and 1.4 × 10⁹ cells/cm², respectively. The increasing sessile cell count trend agrees with the decreasing dissolved [H₂S] in Table 2. Decreased [H₂S] means less toxicity and thus better sessile cell growth.^{12, 24} Although the 300 mL headspace bottle had lower H₂S concentrations in both the gas and the liquid phases, its total amount (1.47 × 10⁻⁴ mol) was higher than in the bottles with 150 mL and 200 mL headspace volumes. This was reasonable because less H₂S toxicity allowed better SRB growth and thus produced more H₂S in the total amount in the liquid and headspace of a sealed anaerobic vial.

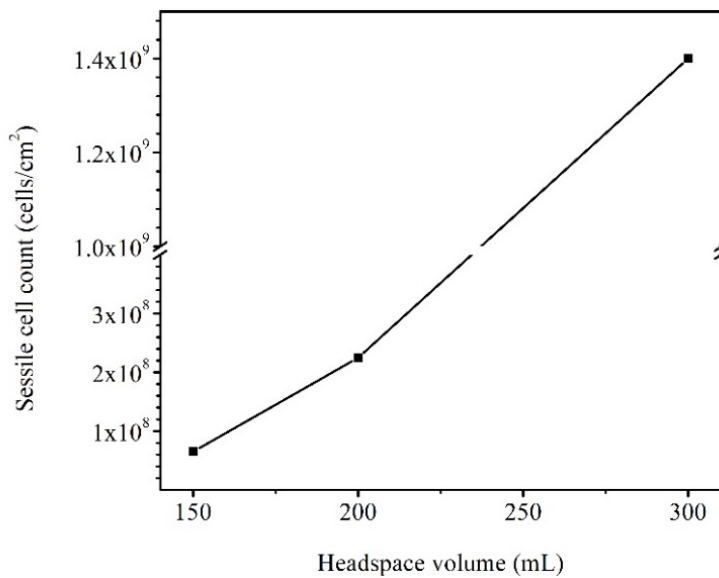


Figure 3. Sessile cell counts on dogbone coupons after 14-day incubation in bottles with fixed 150 mL broth and varied headspace volume.

The weight losses for 150 mL headspace, 200 mL headspace and 300 mL headspace volumes were 1.7 mg/cm², 1.9 mg/cm² and 2.3 mg/cm², respectively (Figure 4). The increasing trend corresponds to the increasing sessile cell trend in Figure 3. More sessile cells for more weight loss is consistent with EET-MIC.

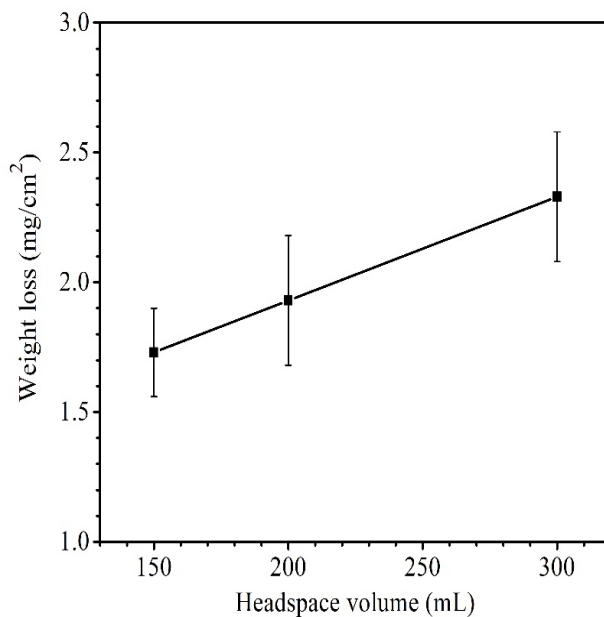


Figure 4. Weight losses of X80 in 150 mL SRB broth with varied headspace volume after 14-day incubation. (Each error bar represents standard deviation from 3 coupons in the same anaerobic bottle.)

Polarization resistance (R_p) from LPR scans in Figure 5 describes the transient corrosion kinetics during the 14-day incubation. Figure 5 shows that R_p for the 300 mL headspace was the lowest. A lower R_p means a higher corrosion rate. This means the largest headspace led to the largest corrosion rate, which is consistent with sessile cell count data in Figure 3 and weight loss data in Figure 4.

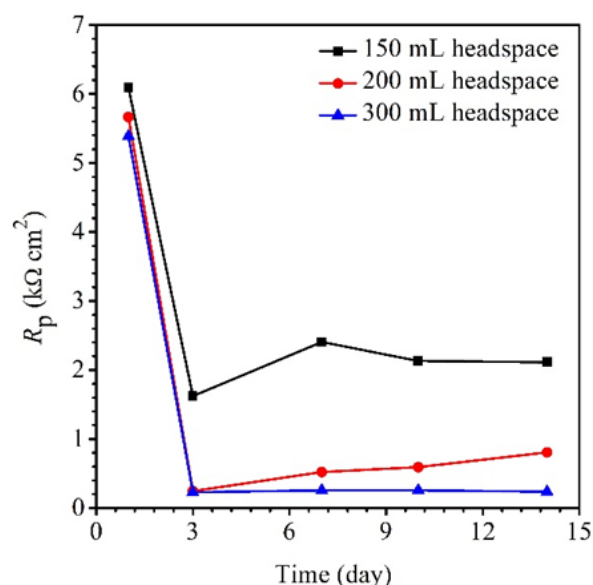
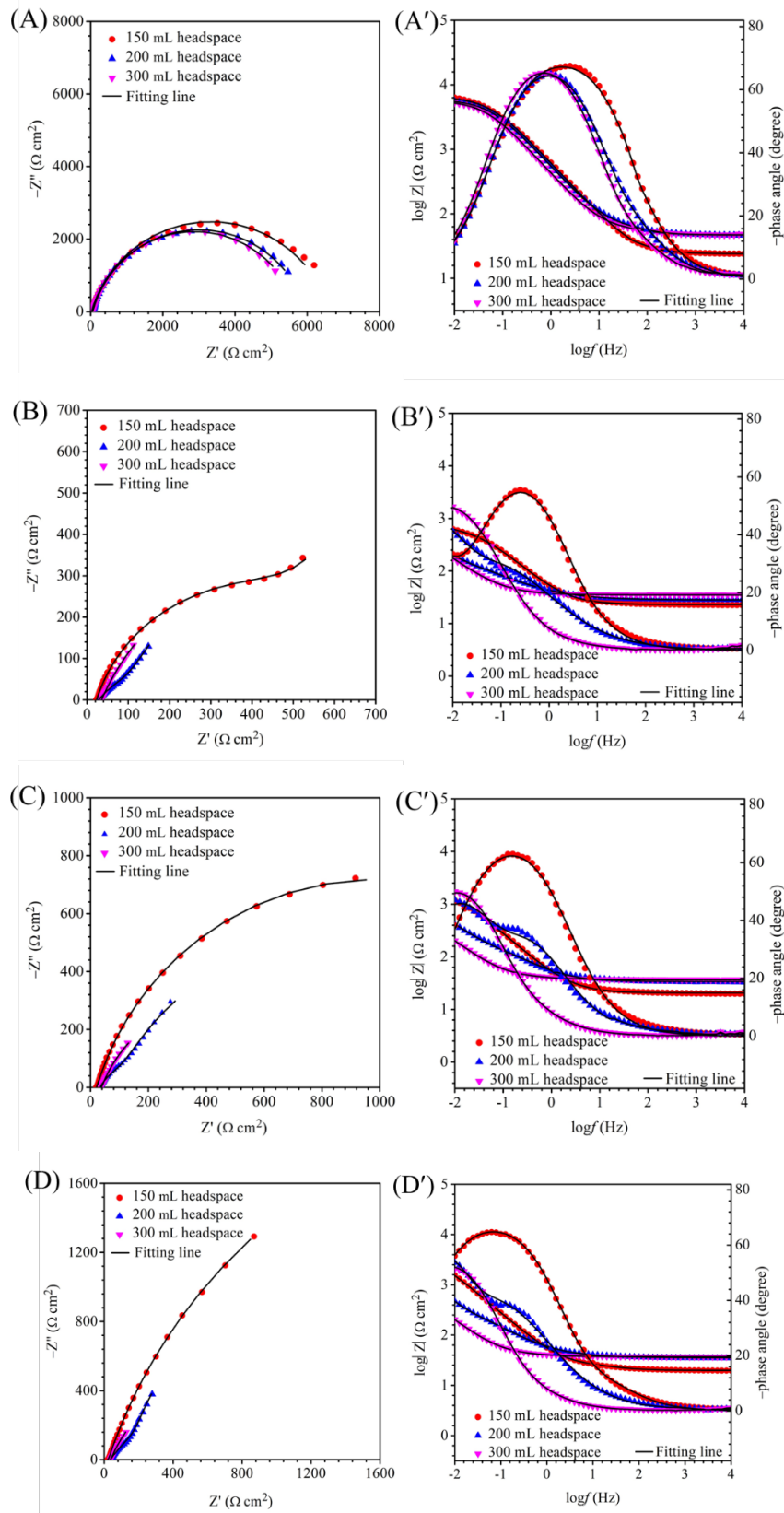


Figure 5. Variations of R_p vs. time in 150 mL SRB broth with varied headspace volume during 14-day incubation

For EIS, the Nyquist and Bode plots of the biotic X80 dogbone coupons for different immersion times and different headspace volumes are shown in Figure 6. The Nyquist plots of the dogbone coupons indicates a capacitive behavior. A larger diameter of the semi-circle in the Nyquist plot means a higher corrosion resistance (Figure 6A, B). The EIS data in Figure 6 were fitted with the equivalent electrical circuit in Figure 7. The fitted parameters are summarized in Table 3. The biotic impedance spectra for three different headspace volumes (150 mL, 200 mL and 300 mL) fitted well with the two-time constant circuit model. The capacitors in the circuit model were not ideal capacitors. Thus, constant phase elements (CPEs) were used instead. The equivalent circuit in Figure 7 contains: (1) solution resistance (R_s), (2) a parallel combination of charge transfer resistance (R_{ct}) and CPE₁ associated with the heterogeneous layer containing the corrosion products layer, (3) a parallel combination of biofilm resistance (R_b) and CPE₂ associated with the biofilm layer on the X80 steel surface.

Electrochemical parameters from EIS modeling are shown in Table 3. Compared with charge resistance (R_{ct}) values, the film resistance R_b values are quite small. However, the R_b values became larger with the increasing headspace volumes due to *D. vulgaris* growing better under the larger headspace, which is consistent with the increased sessile cell count (Figure 4). R_{ct} was rating limiting in this study. ($R_{ct} + R_b$) is the smallest for 300 mL headspace in Table 3, indicating the highest corrosion rate.

The Tafel plots of X80 in the SRB broth are shown in Figure 8. The corrosion current densities from a Tafel analysis of the potentiodynamic polarization curves are listed in Table 4. The coupon for the 300 mL headspace shows the highest corrosion current density (i_{corr}) of $74.8\ \mu\text{A}/\text{cm}^2$ (Figure 8, Table 4) after 14 days of incubation, compared to those for 150 mL ($4.8\ \mu\text{A}/\text{cm}^2$) and 200 mL ($19.1\ \mu\text{A}/\text{cm}^2$) headspace volumes. The corrosion current density trend here corroborates the $1/R_p$ (Figure 5) and $1/(R_{ct} + R_b)$ (Table 3) data trends. Their corrosion trends are consistent with weight loss and pit depth data trends, all pointing to more sessile cells for faster MIC.



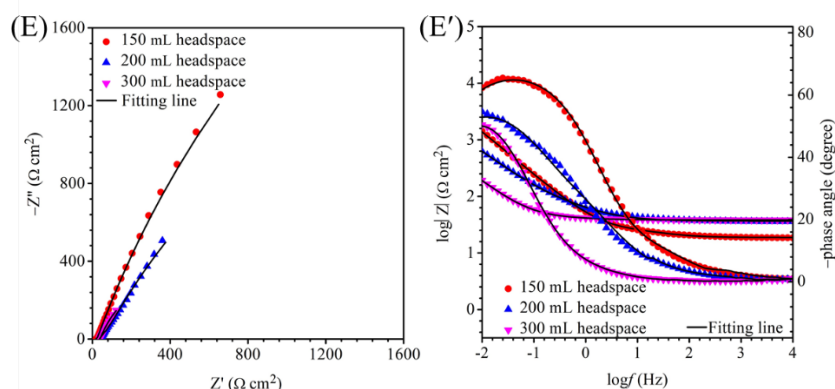


Figure 6. Nyquist and Bode plots for X80 in SRB broth during 14-day incubation with fixed 150 mL broth with varied headspace volume: (A, A') 1st day, (B, B') 4th day, (C, C') 7th day, (D, D') 10th day and (E, E') 14th day.

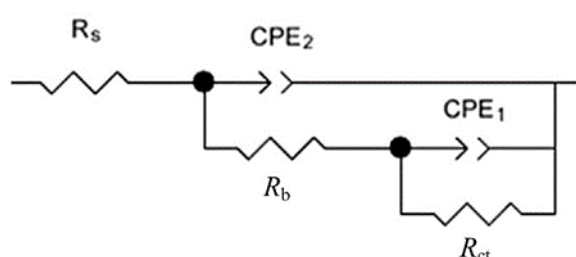


Figure 7. Equivalent circuit for fitting EIS spectra in Figure 6.

**Table 3
Electrochemical parameters obtained from fitting EIS spectra in Figure 9.**

Headspace (mL)	Day	R_s ($\Omega \text{ cm}^2$)	Y_2 ($\Omega^{-1} \text{ cm}^{-2} \text{ s}^n$)	n_2	R_b ($\Omega \text{ cm}^2$)	Y_1 ($\Omega^{-1} \text{ cm}^{-2} \text{ s}^n$)	n_1	R_{ct} ($\text{k}\Omega \text{ cm}^2$)
150	1	24	1.41×10^{-4}	0.89	4	1.01×10^{-3}	0.71	6.78
	3	20	4.76×10^{-3}	0.78	11	1.14×10^{-3}	0.97	1.91
	7	18	5.11×10^{-3}	0.74	12	3.24×10^{-3}	0.87	5.76
	10	19	5.24×10^{-3}	0.73	12	2.07×10^{-3}	0.97	9.87
	14	24	4.03×10^{-3}	0.78	7	6.13×10^{-3}	0.88	9.98
200	1	47	1.01×10^{-4}	0.88	41	1.47×10^{-3}	0.80	5.88
	3	28	1.51×10^{-3}	0.63	121	2.40×10^{-3}	0.68	2.21
	7	34	7.62×10^{-3}	0.72	180	1.13×10^{-2}	0.71	1.32
	10	36	8.07×10^{-3}	0.68	259	9.11×10^{-3}	0.76	4.87
	14	37	7.04×10^{-3}	0.64	129	2.93×10^{-3}	0.75	5.63
300	1	47	1.83×10^{-4}	0.85	39	1.85×10^{-3}	0.84	5.63
	3	35	4.51×10^{-3}	0.74	152	2.36×10^{-3}	0.93	0.94
	7	37	3.80×10^{-3}	0.75	115	6.38×10^{-3}	0.92	0.86
	10	37	3.73×10^{-3}	0.74	88	7.43×10^{-3}	0.98	1.16
	14	38	3.31×10^{-3}	0.76	17	1.41×10^{-2}	0.80	0.96

The Tafel plots of X80 in the SRB broth are shown in Figure 8. The corrosion current densities from a Tafel analysis of the potentiodynamic polarization curves are listed in Table 4. The coupon for the 300 mL headspace shows the highest corrosion current density of $74.8 \mu\text{A}/\text{cm}^2$ (Figure 8, Table 4) after 14 days of incubation, compared to those for 150 mL ($4.8 \mu\text{A}/\text{cm}^2$) and 200 mL ($19.1 \mu\text{A}/\text{cm}^2$) headspace volumes. The corrosion current density trend here corroborates the $1/R_p$ (Figure 5) and $1/(R_{ct} + R_b)$ (Table 3) data trends. These corrosion trends are all consistent with weight loss and pit depth data trends, all pointing to more sessile cells for faster MIC.

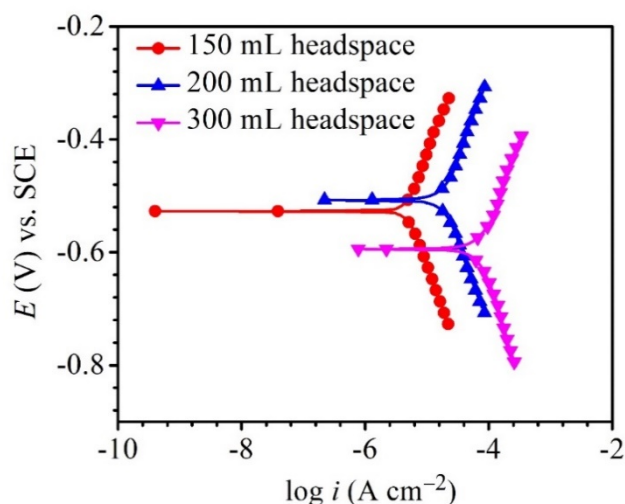


Figure 8. Potentiodynamic polarization curves at end of 14-day incubation.

Table 4
Fitted electrochemical parameters from Tafel analysis at the end of the 14-day incubation.

Headspace (mL)	i_{corr} ($\mu\text{A}/\text{cm}^2$)	E_{corr} (mV) vs. SCE	β_a (mV/dec)	β_c (mV/dec)
150	4.8	-550	314	-299
200	19.1	-520	328	-322
300	74.8	-590	387	-279

Fe^{2+} can be precipitated by the following reaction when FeS is supersaturated in the broth,^{9, 10}



Due to the headspace volume change, there was less FeS precipitation with a larger headspace because it had less dissolved $[\text{H}_2\text{S}]$, and thus the broth was less dark.^{9, 13} In this work, smaller $[\text{H}_2\text{S}]$ in the broth led to better sessile cell growth and thus more severe EET-MIC. This is in agreement with the observation made by Jia et al.¹² Jia et al. further demonstrated that the presence of Fe^{2+} in the ATCC[†] 1249 culture medium serves the function of detoxifying H_2S to compensate for sulfide precipitation of Fe^{2+} which is a key enzyme co-factor for SRB growth.¹³ In their experimental design with broth volume and headspace volume both fixed, they showed that adding more Fe^{2+} in the medium led to a higher sessile cell count and a higher $[\text{H}_2\text{S}]$ and thus more FeS precipitation. In the headspace variation and Fe^{2+} variation experiments, $[\text{H}_2\text{S}]$, FeS precipitation trends were opposite in relation to weight loss trend. Thus, using $[\text{H}_2\text{S}]$, FeS precipitation to predict MIC outcome can be erroneous. However, in both cases, sessile cell count increase correlated with increased weight loss. Thus, H_2S should not be a major contributor in the SRB MIC of carbon steel for broth near neutral pH. This is in agreement with Jia et al.^{12, 13}

Coupon surface morphologies on dogbone coupons after the 14-day incubation with biofilms and corrosion products removed were examined under IFM. Figure 9(a) shows that the abiotic coupon surface exhibits polished coupon surface roughness (y-scale enlarged to show details). For the biotic dogbone coupons, the maximum pit depth increased with a larger headspace volume as shown in Figure 9(b) to Figure 9(d). They were 2.6 μm , 4.2 μm and 6.2 μm for headspace volumes of 150 mL, 200 mL and 300 mL, respectively. The pit depth trend here is consistent with the weight loss data trend. With a larger headspace, there was a lower amount of dissolved $[\text{H}_2\text{S}]$ and more sessile cells, which led to more severe weight loss and deeper pits. The maximum pit depth increased by 58% when the headspace increased from 150 mL to 300 mL, while the broth volume was fixed at 150 mL.

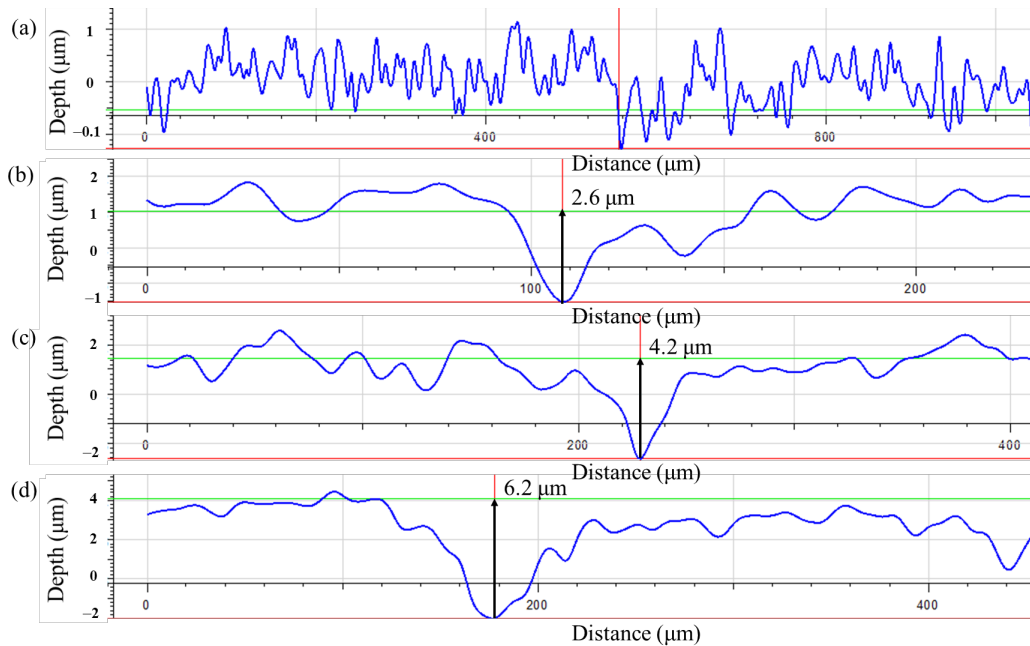


Figure 9. Maximum pit depths on dogbone coupons after 14-day incubation in bottles with headspace volumes of: (a) 150 mL (abiotic control), (b) 150 mL, (c) 200 mL, and (d) 300 mL, respectively.

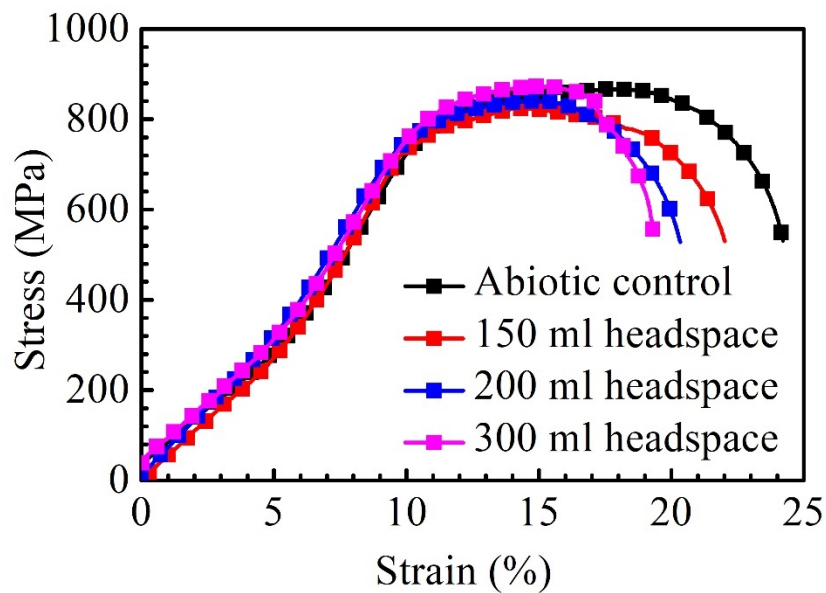


Figure 10. Stress–strain curves obtained after 14-day incubation with SRB, and for the abiotic dogbone.

Figure 10 shows the stress-strain curves of X80 dogbone coupons which were retrieved after they had been immersed in bottles with fixed 150 mL culture medium and varied headspace volumes (150 mL, 200 mL and 300 mL) for 14 days. The ultimate (tensile) strength is the maximum stress that a material can withstand before final failure, which is the highest point of the Y-axis in Figure 10. The ultimate strain (elongation at break) can demonstrate the ability of a material to resist shape change before finally breaking. It is the largest value of the X-axis (strain) in Figure 10.²⁰ Lowering of these parameters can reflect the mechanical property degradation of the material under different conditions such as different MIC severity. The ultimate strength of abiotic control X80 carbon steel was 866 MPa. The ultimate tensile

strength values of for the abiotic coupon and biotic dogbone coupons from bottles with different headspace volumes were all quite close as shown in Figure 10. Compared with the abiotic dogbone, in the presence of SRB with headspace volumes of 150 mL, 200 mL 300 mL, the ultimate strength loss was only 5%, 3% and 0%, respectively. These values were rather small. Ultimate strain was reduced in the presence of SRB. Compared with the abiotic dogbone, in the presence of SRB with headspace volumes of 150 mL, 200 mL 300 mL, the ultimate strain losses were 19%, 20% and 22%, respectively. With an increasing headspace, MIC severity increased, making X80 steel more brittle. The corrosion damage by SRB pitting was the main factor in its mechanical property degradation study. H₂S was unlike the driving force behind the relatively large ultimate strain loss, because in this work, more severe MIC corresponded with lower [H₂S] in the broth.

CONCLUSIONS

1. The tensile testing results show that the presence of SRB made the X80 steel more brittle which was reflected by the relatively large ultimate strain losses, compared to the abiotic control. Meanwhile, the ultimate strength loss was small for all the dogbone coupons after 14 days of incubation.
2. More severe MIC weight loss and pitting led to more ultimate strain loss in X80.
3. This work confirms that in an anaerobic bottle with SRB, a larger headspace allows more H₂S to escape from the broth, and this reduces the H₂S toxicity in the broth and thus promoting SRB growth. Increased sessile cell count leads to more severe weight loss and MIC pitting, which is consistent with EET-MIC.

ACKNOWLEDGEMENTS

We acknowledge the financial support from Saudi Aramco, PTTEP of Thailand and Chinese Society for Corrosion and Protection (CSCP).

REFERENCES

1. P. Elliott, S. Ragusa, D. Catcheside. (1998). Growth of Sulfate-Reducing Bacteria under Acidic Conditions in an Upflow Anaerobic Bioreactor as a Treatment System for Acid Mine Drainage. *Water Research*, 32(12), 3724-3730.
2. D. Walsh, D. Pope, M. Danford, T. Huff. (1993). The Effect of Microstructure on Microbiologically Influenced Corrosion. *JOM*, 45(9), 22-30.
3. D. Enning, J. Garrelfs. (2014). Corrosion of Iron by Sulfate-Reducing Bacteria: New Views of an Old Problem. *Applied and environmental microbiology*, 80(4), 1226-1236.
4. D.R. Lovley, E.J. Phillips. (1994). Novel Processes for Anaerobic Sulfate Production from Elemental Sulfur by Sulfate-Reducing Bacteria. *Applied and Environmental Microbiology*, 60(7), 2394-2399.
5. D. Xu, T. Gu. (2014). Carbon Source Starvation Triggered More Aggressive Corrosion against Carbon Steel by the *Desulfovibrio vulgaris* Biofilm. *International Biodeterioration & Biodegradation*, 91, 74-81.
6. D. Xu, Y. Li, T. Gu. (2016). Mechanistic Modeling of Biocorrosion Caused by Biofilms of Sulfate Reducing Bacteria and Acid Producing Bacteria. *Bioelectrochemistry*, 110, 52-58.
7. R.K. Thauer, E. Stackebrandt, W.A. Hamilton. (2007). Energy Metabolism and Phylogenetic Diversity of Sulphate-Reducing Bacteria. *Sulphate-reducing bacteria: Environmental and engineered systems*, 1-37.
8. W. Dou, J. Liu, W. Cai, D. Wang, R. Jia, S. Chen, T. Gu. (2019). Electrochemical Investigation of Increased Carbon Steel Corrosion Via Extracellular Electron Transfer by a Sulfate Reducing Bacterium under Carbon Source Starvation. *Corrosion Science*, 150, 258-267.
9. D. Wang, J. Liu, R. Jia, W. Dou, S. Kumseranee, S. Punpruk, X. Li, T. Gu. (2020). Distinguishing

- Two Different Microbiologically Influenced Corrosion (MIC) Mechanisms Using an Electron Mediator and Hydrogen Evolution Detection. *Corrosion Science*, 177, 108993, <https://doi.org/10.1016/j.corsci.2020.108993>.
10. T. Gu, R. Jia, T. Unsal, D. Xu. (2019). Toward a Better Understanding of Microbiologically Influenced Corrosion Caused by Sulfate Reducing Bacteria. *Journal of materials science & technology*, 35(4), 631-636.
 11. T. Gu, D. Xu, "Why Are Some Microbes Corrosive and Some Not?" CORROSION NACE International, 2013.
 12. R. Jia, J.L. Tan, P. Jin, D.J. Blackwood, D. Xu, T. Gu. (2018). Effects of Biogenic H₂S on the Microbiologically Influenced Corrosion of C1018 Carbon Steel by Sulfate Reducing *Desulfovibrio vulgaris* Biofilm. *Corrosion Science*, 130, 1-11.
 13. R. Jia, D. Wang, P. Jin, T. Unsal, D. Yang, J. Yang, D. Xu, T. Gu. (2019). Effects of Ferrous Ion Concentration on Microbiologically Influenced Corrosion of Carbon Steel by Sulfate Reducing Bacterium *Desulfovibrio vulgaris*. *Corrosion Science*, 153, 127-137.
 14. T. Unsal, E. Ilhan-Sungur, S. Arkan, N. Cansever. (2016). Effects of Ag and Cu Ions on the Microbial Corrosion of 316L Stainless Steel in the Presence of *Desulfovibrio* Sp. *Bioelectrochemistry*, 110, 91-99.
 15. J. Sheng, J. Xia. (2017). Effect of Simulated Pitting Corrosion on the Tensile Properties of Steel. *Construction and Building Materials*, 131, 90-100.
 16. S. Saad-Eldeen, Y. Garbatov, C.G. Soares. (2012). Effect of Corrosion Degradation on Ultimate Strength of Steel Box Girders. *Corrosion engineering, science and technology*, 47(4), 272-283.
 17. R. Javaherdashti. (2011). Impact of Sulphate-Reducing Bacteria on the Performance of Engineering Materials. *Applied microbiology and biotechnology*, 91(6), 1507.
 18. R. Vaidya, D. Butt, L. Hersman, A. Zurek. (1997). Effect of Microbiologically Influenced Corrosion on the Tensile Stress-Strain Response of Aluminum and Alumina-Particle Reinforced Aluminum Composite. *Corrosion*, 53(2), 136-141.
 19. M. Yousaf, I. Ali, M. Arif, G. Mustafa, S. Ahmad, N. Afzal, I. Ghauri. (2015). Effects of Microbiologically Influenced Corrosion by *Bacillus Megaterium* Bacteria on the Mechanical Properties of Al-Cu Alloy. *Materials Today: Proceedings*, 2(10), 5669-5673.
 20. Służalec, A. (1992). Stress-Strain Curve. In: Introduction to Nonlinear Thermomechanics (pp. 45-47). Springer, London.
 21. ASTM G30-97. (2000). Standard Practice for Making and Using U-Bend Stress-Corrosion Test Specimens.
 22. J. Ning, Y. Zheng, D. Young, B. Brown, S. Nešić. (2014). Thermodynamic Study of Hydrogen Sulfide Corrosion of Mild Steel. *Corrosion*, 70(4), 375-389.
 23. W. Sun, S. Nestic. (2007). A Mechanistic Model of H₂S Corrosion of Mild Steel. *CORROSION 2007*.
 24. R. Jia, D. Yang, W. Dou, J. Liu, A. Zlotkin, S. Kumseranee, S. Punpruk, X. Li, T. Gu. (2019). A Sea Anemone-Inspired Small Synthetic Peptide at Sub-Ppm Concentrations Enhanced Biofilm Mitigation. *International Biodeterioration & Biodegradation*, 139, 78-85.